

Magnetization reversal of ferromagnetic nanodisk placed above a superconductor

A. A. Fraerman^{1,2}, I. R. Karetnikova, I. M. Nefedov, I. A. Shereshevskii, and M. A. Silaev

¹ *Institute for Physics of Microstructures, Russian Academy of Sciences, 603950, Nizhny Novgorod, GSP-105, Russia,*

² *Argonne National Laboratory, Argonne, Illinois, 60439*

(Dated: October 27, 2018)

Using numerical simulation we have studied a magnetization distribution and a process of magnetization reversal in nanoscale magnets placed above a superconductor plane. In order to consider an influence of superconductor on magnetization distribution in the nanomagnet we have used London approximation. We have found that for usual values of London penetration depth the ground state magnetization is mostly unchanged. But at the same time the fields of vortex nucleation and annihilation change significantly: the interval where vortex is stable enlarges on 100-200 Oe for the particle above the superconductor. Such fields are experimentally observable so there is a possibility of some practical applications of this effect.

PACS numbers: 75.75.+a, 75.60.Jk, 74.81.-g

I. INTRODUCTION

In the past few years considerable attention has been devoted to the investigations of magnetism in small nanosized ferromagnetic particles. Such interest is caused by the opportunities for creating recording devices¹⁻³ and ultrasmall magnetic field sensors⁴ based on the properties of ferromagnetic particles. It is now well-understood that magnetization distribution in a single particle is determined by the competition between the magnetostatic and exchange energies. If a particle is small, it is uniformly magnetized and if its size is large enough a non-uniform(vortex) magnetization is more energy preferable(see, for example, Refs. 4, 5, 6, 7). Besides the geometrical form and size, the state of the particle depends on many other factors. For example, by applying a homogeneous magnetic field we can cause nucleation or annihilation of the vortex. In an array of particles their magnetostatic interaction may have a strong influence on a particle magnetization. If the distance between particles is rather small then magnetostatic interaction has a strong destabilizing effect on the vortex state, leading to a significant decrease in both the nucleation and annihilation fields^{8,9}.

The interplay between the ferromagnetism and superconductivity can also lead to changes in the magnetization distribution. It was shown that in a ferromagnetic film put on a superconducting substrate the size of the domains is up to $\sqrt{1.5}$ times smaller than for a film without a superconducting substrate^{10,11}. The experimental investigations revealed changes in the magnetic field around Al/Ni submicron structures with a decrease in the temperature to values below T_c . This effect was referred to the expulsion of the magnetic field by the superconducting part of the Ferromagnetic/Superconductor (FS) hybrid structures¹².

All investigations of the FS interaction deal with the changes of the ferromagnetic domain structure. Therefore the results thereof cannot be applied to the single-domain nanoparticles. On the one hand, the magnetization of a nanoparticle is more simple than the domain

structure of a macroscopic ferromagnetic, therefore, theoretical findings could be proved by experiments with nanoparticles. But on the other hand, the magnitude of the interaction between the nanoparticles and the superconductor is strongly reduced due to the large values of the London penetration depth.

In this work we investigate the phase transition between the single-domain and the vortex state, and the process of magnetization reversal of a ferromagnetic nano-sized particle placed above the surface of a superconductor. The superconducting state is described using the London approximation, that is, we assume that the particle cannot produce a vortex- antivortex pair. This assumption is not universally true, since if the particle dimensions are sufficiently large its magnetic field can destroy the Meijssner state of the superconductor¹³. The criteria of the London approximation applicability can be obtained in the following way. The largest magnetic field is generated by a single-domain particle. Then, the maximal magnetic flux through the surface of a superconductor is $\phi_m = \pi R h M$, where R and h are the radius and the height of the particle and M is the magnetization. The flux ϕ_m must be less than the flux quantum $\phi_0 = 2,07 \cdot 10^{-7} \text{gs} \cdot \text{sm}^2$ in order to exclude the possibility of a vortex penetration. We consider a ferromagnetic particle with a saturation magnetization of about $M_s = 800 \text{oe}$. Then we have the following limitation on the particle dimensions: $Rh < 8 \cdot 10^3 \text{nm}^2$. So we consider only the particles which obey this condition.

The equilibrium distribution of magnetization which gives a minimum to the energy functional is found by numerical simulation. For numerical simulation we use the approach based on the Landau-Lifshitz-Gilbert(LLG) equation for the dynamics of magnetic moments. This approach enables us to investigate metastable states which realize the local minimums of the energy functional. The metastable states are of great importance since the finiteness of the nucleation and annihilation fields values is the consequence of the energy barrier between single-domain and vortex-like states. We obtain a phase diagram of the particle in the height/diameter

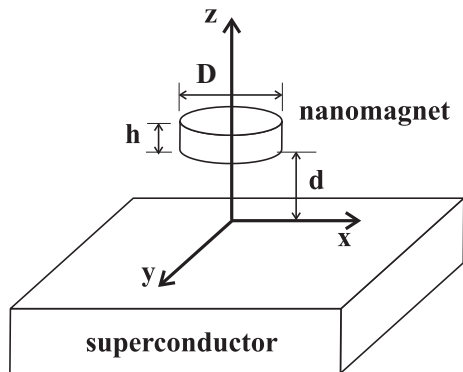


FIG. 1: Ferromagnetic nanoparticle above the surface of superconductor.

plane for the transition from the single-domain to the vortex-like state. We find that for the realistic value of the London penetration depth the FS interaction is rather weak. The energy of the FS interaction is about 100 times smaller than the self energy of the particle. Therefore, the FS interaction has no influence on the phase diagram. Nevertheless, the magnetization curve of the particle in an external homogeneous magnetic field changes significantly. Even the 1/100 energy shift means that the superconducting screening current produces a magnetic field of about $4\pi M/100 \sim 100Oe$ which leads to experimentally observable decrease of the vortex nucleation field and increase of the annihilation field. The paper is organized as follows. In Sec.2 we derive the analytical expression for the energy functional of our system. In Sec.3 we show the most important features of the numerical simulation. In Sec.4 we discuss the results and also propose possible experiments. Finally, the summary is given in Sec.5.

II. ENERGY FUNCTIONAL

The system we consider is a ferromagnetic particle placed above the surface of a superconductor (Fig.1). We assume that the superconductor occupies the whole half-space, so it has only one boundary plane, $z = 0$. The ferromagnetic particle is assumed to be made of soft magnetic material, so the energy of anisotropy is equal to zero. The total energy of the system of particle and superconductor reads:

$$E = E_e + E_m + E_{ext}. \quad (1)$$

The first term E_e is the energy of the exchange interaction:

$$E_e = -\frac{J}{2M_s^2} \int_V (|\nabla M_x|^2 + |\nabla M_y|^2 + |\nabla M_z|^2) d^3\mathbf{r}, \quad (2)$$

where J is the constant of exchange interaction. The second term E_m in Eq.(1) is the magnetostatic energy¹⁶:

$$E_m = -\frac{1}{2} \int_V \mathbf{H} \cdot \mathbf{M} d^3\mathbf{r}. \quad (3)$$

Here \mathbf{H} is the sum of magnetic field \mathbf{H}_m induced by the particle and magnetic field \mathbf{H}_s generated by the superconducting current:

$$\mathbf{H} = \mathbf{H}_m + \mathbf{H}_s.$$

The last term E_{ext} in Eq.(1) is the energy of the interaction between the magnetic moment and the external field \mathbf{H}_0 :

$$E_{ext} = - \int_V \mathbf{H}_0 \cdot \mathbf{M} d^3\mathbf{r}. \quad (4)$$

In order to obtain the energy as the functional of \mathbf{M} we should express the magnetic field \mathbf{H} in terms of \mathbf{M} . To this end we should solve the Maxwell-London equations where the source is a magnetic current $\mathbf{j}_m = c\nabla \times \mathbf{M}$.

In the space outside the superconductor the system is described by the following equations:

$$\nabla \times \mathbf{B} = \frac{4\pi}{c} \mathbf{j}_m \quad (5)$$

$$\nabla \cdot \mathbf{B} = 0 \quad (6)$$

where we introduce the vector of magnetic induction $\mathbf{B} = \mathbf{H} + 4\pi\mathbf{M}$. The superconductor is described by the equations:

$$\nabla \times \mathbf{B} = \frac{4\pi}{c} \mathbf{j}_s \quad (7)$$

$$\mathbf{B} = -\lambda_L^2 \frac{4\pi}{c} \nabla \times \mathbf{j}_s, \quad (8)$$

where \mathbf{j}_s is the superconducting current and λ_L is the London penetration depth. For the boundary conditions we take the continuity of the magnetic induction \mathbf{B} and its derivatives at the boundary plane $z = 0$. Since the Maxwell-London equations are linear, we first can consider a single magnetic dipole placed at the point $\mathbf{r}_0 = (x_0, y_0, z_0)$ above the surface of the superconductor:

$$\mathbf{M} = \mathbf{m}\delta(\mathbf{r} - \mathbf{r}_0),$$

where \mathbf{m} is the magnetic dipole moment. Once this problem is solved, we can construct the solution for any magnetization distribution. After a bit troublesome but straightforward computation, we obtain the solution to

the single-dipole problem at the half-space $z > 0$ in the form:

$$\mathbf{B} = -\nabla\phi + 4\pi\mathbf{M},$$

where the magnetic potential ϕ is:

$$\phi = \phi_d + \phi_{refl} + \phi_\lambda. \quad (9)$$

The first term ϕ_d in Eq.(9) is the potential of a single magnetic dipole without a superconductor:

$$\phi_d(\mathbf{r}) = -\mathbf{m} \cdot \nabla \frac{1}{|\mathbf{r} - \mathbf{r}_0|},$$

The second term ϕ_{refl} is the potential of the magnetic dipole reflected at the plane $z = 0$:

$$\phi_{refl}(\mathbf{r}) = -\mathbf{m}^* \cdot \nabla \frac{1}{|\mathbf{r} - \mathbf{r}_0^*|},$$

where

$$\mathbf{r}_0^* = (x_0, y_0, -z_0),$$

$$\mathbf{m}^* = (m_x, m_y, -m_z).$$

The third term ϕ_λ in Eq.(9) appears due to the finiteness of the London penetration depth value λ_L . The expression for ϕ_λ is:

$$\phi_\lambda(\mathbf{r}) = -\mathbf{m}^* \cdot \nabla g(\mathbf{r} - \mathbf{r}_0^*), \quad (10)$$

where

$$g(\mathbf{r}) = \lambda_L^2 \int_0^\infty 2k^2 \exp(-kz) J_0(k\rho) dk -$$

$$\lambda_L^2 \int_0^\infty 2k(k^2 + \lambda_L^{-2})^{1/2} \exp(-kz) J_0(k\rho) dk,$$

$$\rho = (x^2 + y^2)^{1/2}.$$

Here $J_0(x)$ is the Bessel function. Then the single dipole magnetic field above the surface of the superconductor is expressed as:

$$\mathbf{B}(\mathbf{r}) = \mathbf{H}(\mathbf{r}) + 4\pi\mathbf{m}\delta(\mathbf{r} - \mathbf{r}_0),$$

$$\mathbf{H}(\mathbf{r}) = \widehat{\mathbf{D}}(\mathbf{r}, \mathbf{r}_0)\mathbf{m}$$

where $\widehat{\mathbf{D}}$ is the modified dipole matrix:

$$\widehat{\mathbf{D}}(\mathbf{r}, \mathbf{r}_0) = \widehat{\mathbf{D}}_d(\mathbf{r} - \mathbf{r}_0) + \widehat{\mathbf{D}}_s(\mathbf{r} - \mathbf{r}_0^*), \quad (11)$$

Here the first term is an ordinary dipole matrix:

$$D_{dx_1x_2}(\mathbf{r}) = \frac{\partial^2}{\partial x_1 \partial x_2} \frac{1}{|\mathbf{r}|},$$

and the second term appears due to the presence of the superconductor

$$D_{sx_1x_2}(\mathbf{r}) = (-1)^{\delta_{z,x_2}} \frac{\partial^2}{\partial x_1 \partial x_2} \left(g(\mathbf{r}) + \frac{1}{|\mathbf{r}|} \right).$$

where indexes x_1 and x_2 denote coordinates x, y, z and δ_{z,x_2} is the Kronecker's symbol.

Let us now consider continuous distribution of the magnetic moment $\mathbf{M}(\mathbf{r})$. The magnetic field generated by the superconducting current is given as a sum of single-dipole solutions:

$$\mathbf{H}_s = \int_V \widehat{\mathbf{D}}_s(\mathbf{r} - \mathbf{r}_0^*) \mathbf{M}(\mathbf{r}_0) d^3\mathbf{r}_0.$$

For the magnetic field \mathbf{H}_m generated by the magnetic current we cannot take the sum of the single-dipole fields since the dipole matrix $\widehat{\mathbf{D}}_d(\mathbf{r})$ has a nonintegrable singularity at point $\mathbf{r} = 0$. Therefore, the expression for \mathbf{H}_m that we use is:

$$\mathbf{H}_m(\mathbf{r}) = - \int_V \nabla \cdot \mathbf{M}(\mathbf{r}_0) \frac{\mathbf{r} - \mathbf{r}_0}{|\mathbf{r} - \mathbf{r}_0|^3} d^3\mathbf{r}_0 +$$

$$\int_{\partial V} (\mathbf{M}(\mathbf{r}_0) \cdot \mathbf{n}_s(\mathbf{r}_0)) \frac{\mathbf{r} - \mathbf{r}_0}{|\mathbf{r} - \mathbf{r}_0|^3} d^3\mathbf{r}_0.$$

Here, $V, \partial V$ are the volume and surface of a particle and \mathbf{n}_s is the unit vector of the external normal to the surface at a current point.

Finally, we consider the energy functional consisting of the self-energy of particle E_0 , the energy of interaction with the superconductor E_{int} and with external field E_{ext} :

$$E = E_0 + E_{int} + E_{ext}.$$

Self-energy E_0 includes exchange E_e energy and the part E_d of magnetostatic energy E_m :

$$E_0 = E_e + E_d,$$

where

$$E_d = -\frac{1}{2} \int_V \mathbf{H}_m \cdot \mathbf{M} d^3\mathbf{r} =$$

$$-\frac{1}{2} \int_{V \times V} (\nabla \cdot \mathbf{M}(\mathbf{r})) (\nabla \cdot \mathbf{M}(\mathbf{r}')) \frac{d^3\mathbf{r} d^3\mathbf{r}'}{|\mathbf{r} - \mathbf{r}'|}$$

$$+\frac{1}{2}\int_{V\times\partial V}(\nabla\cdot\mathbf{M}(\mathbf{r}'))(\mathbf{M}(\mathbf{r})\cdot\mathbf{n}_s)\frac{d^3\mathbf{r}d^3\mathbf{r}'}{|\mathbf{r}-\mathbf{r}'|}$$

$$-\frac{1}{2}\int_{\partial V\times\partial V}(\mathbf{M}(\mathbf{r}')\cdot\mathbf{n}'_s)(\mathbf{M}(\mathbf{r})\cdot\mathbf{n}_s)\frac{d^3\mathbf{r}d^3\mathbf{r}'}{|\mathbf{r}-\mathbf{r}'|}.$$

The energy of interaction E_{int} of the particle with the superconductor is the energy of the magnetic moment in the field produced by the superconducting current, and it is the other part of the magnetostatic energy E_m :

$$E_{int} = -\frac{1}{2}\int_V \mathbf{H}_s \cdot \mathbf{M} d^3\mathbf{r} =$$

$$-\frac{1}{2}\int_{V\times V} \mathbf{M}(\mathbf{r}) \cdot \hat{\mathbf{D}}_s(\mathbf{r}, \mathbf{r}_0) \mathbf{M}(\mathbf{r}_0) d^3\mathbf{r} d^3\mathbf{r}_0$$

The energy E_{ext} is the same as in Eq.(1) and is given by Eq.(4).

III. NUMERICAL SIMULATION

To perform numerical calculation we use the same approach as in Refs. 9 and 14. The basis of our numerical simulation is the LLG equation for magnetization $\mathbf{M}(\mathbf{r}, t)$ of a particle in the form

$$\frac{\partial \mathbf{M}}{\partial t} = -\frac{\gamma}{1+\alpha^2}[\mathbf{M}, \mathbf{H}_{eff}] - \frac{\alpha\gamma}{(1+\alpha^2)M_s}[\mathbf{M}, [\mathbf{M}, \mathbf{H}_{eff}]],$$
(12)

where γ is the gyromagnetic ratio, α is the dimensionless damping parameter and t is time. The effective field \mathbf{H}_{eff} is a variation derivative of the energy functional:

$$\mathbf{H}_{eff} = -\frac{\delta E}{\delta \mathbf{M}}$$

The important feature of the LLG equation is that it describes the evolution of the magnetization distribution to the equilibrium. By varying the initial conditions we find different equilibrium states of our system. Then we choose the equilibrium state with the minimal energy to obtain the ground state. Choosing as the initial state the vortex-like or single-domain distribution and varying the external field \mathbf{H}_0 we determine the vortex annihilation or nucleation field as the critical field of transformation of the vortex-like to single-domain state or vice versa.

To avoid a three-dimensional grid problem to be solved which needs large computer resources we assume that magnetization of a cylindrical particle does not depend on the coordinate z along the cylindrical axis. Then we integrate the relations for the energy over z and z_0 and obtain the energy as a functional of the magnetization which is a function of only two space variables. Then we define the effective field \mathbf{H}_{eff} as a variation derivative of

the obtained functional. The effective field does not depend on z either, so we have a three-dimensional problem reduced to the two-dimensional one.

To develop a numerical method we divide the particle into rectangular parallelepipeds with a square base of size a in the plane (x, y) and of height h and obtain approximate expressions for different parts of the energy functional using the grid values of magnetization $\mathbf{M} = (M_x(\rho), M_y(\rho), M_z(\rho))$.

The expression for the magnetostatic energy E_d reads:

$$E_d[\mathbf{M}] = -\frac{a^4}{2}\sum_{\rho\neq\rho'}\mathbf{M}(\rho')\cdot\hat{\mathbf{D}}_d^h(\rho-\rho')\mathbf{M}(\rho)+E_d^0, \quad (13)$$

where $\rho = (x, y)$ are the points of the square grid with step a on the (x, y) plane and matrix $\hat{\mathbf{D}}_d^h$ is the dipole matrix $\hat{\mathbf{D}}_d$ integrated over the z coordinate:

$$\hat{\mathbf{D}}_d^h(\rho) = \int_0^h dz \int_{-z}^{h-z} \hat{\mathbf{D}}_d(\rho, z') dz'.$$

The additional term E_d^0 in Eq.(13) appears as the contribution of self-interaction in the cell. It depends only on the value of magnetization which is assumed constant, so it does not influence the effective field.

The expression for the exchange energy reads:

$$E_e[\mathbf{M}] = -\frac{Jh}{2M_s^2}\sum_{\rho}\sum_{\rho'}|\mathbf{M}(\rho)-\mathbf{M}(\rho')|^2. \quad (14)$$

The internal summation in Eq.(14) is taken over all neighbors ρ' of the point ρ .

The energy E_{ext} and the interaction energy E_{int} are, respectively:

$$E_{ext} = -a^2h\sum_{\rho}\mathbf{H}_0\cdot\mathbf{M}(\rho); \quad (15)$$

$$E_{int}[\mathbf{M}] = -\frac{a^4}{2}\sum_{\rho\neq\rho'}\mathbf{M}(\rho')\cdot\hat{\mathbf{D}}_s^h(\rho-\rho')\mathbf{M}(\rho), \quad (16)$$

where matrix $\hat{\mathbf{D}}_s^h$ is

$$\hat{\mathbf{D}}_s^h(\rho) = \int_d^{d+h} dz \int_{z+d}^{z+d+h} \hat{\mathbf{D}}_s(\rho, z') dz'.$$

We choose the cell size considering two factors. On one hand the size of the cell should be smaller than the characteristic exchange interaction length ($\sqrt{J/M_s^2}$) in order to describe the inhomogeneous magnetization correctly. On the other hand, we cannot choose it very small because of the computation time limitations.

IV. RESULTS AND DISCUSSION

For computation we choose the following parameters: the saturation magnetization $M_s = 800Oe$, the exchange interaction constant $J = 10^{-6}erg/sm$. The cell size is $3nm \times 3nm$, while the exchange interaction length is approximately $13nm$. The distance d and the London penetration depth have a strong influence on the interaction between a particle and a superconductor. For superconductors with $\lambda_L \sim 50 - 100nm$ the interaction should be largely reduced, since such values of λ_L are comparable to the size of the particle. To compensate for this reduction we can make the distance d small. We choose $\lambda = 50nm$ and $d = 5nm$ since such values are experimentally obtainable and make the effect of a particle-superconductor interaction quite distinctive.

First of all, we investigate how the energy of the interaction between the particle and the superconductor depends on the value of λ_L . We calculate the interaction energy E_{int} for the particle with a single-domain and vortex-like magnetization (Fig.2). The dimensions of the particle are: $h = 10nm$ and $D = 50nm$. The self-energy of this particle is $E_0 = 1.2122 \cdot 10^{-11}erg$ for the single domain state and $E_0 = 1.8856 \cdot 10^{-11}erg$ for the vortex one. The interaction energy decreases rapidly when λ_L changes from 0 to 30–40nm. For larger values of λ_L the interaction energy tends to zero asymptotically. At practically interesting values $\lambda_L \sim 50 - 100nm$ the interaction energy is about $E_{int} \sim 0.0268 \cdot 10^{-11}erg$ for the single-domain magnetization and $E_{int} \sim 0.0014 \cdot 10^{-11}erg$ for the vortex-like magnetization. Thus the interaction with a superconductor is much stronger for a single-domain particle. This is easily understood because the vortex-like magnetization produces a much weaker magnetic field than the single-domain magnetization. The interaction energy for the real values of $\lambda_L \sim 50nm$ is much smaller than the particle self energy: for the single-domain magnetization it is $E_{int}/E_0 \sim 0.02$.

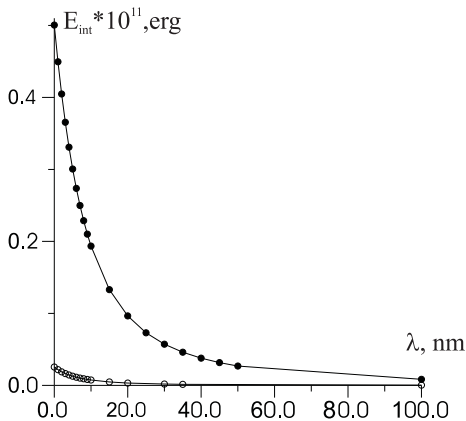


FIG. 2: The energy of interaction of a single-domain (filled circles) and vortex-like (open circles) magnetized particle with a superconductor as a function of λ_L .

Then we study the ground state of the particle inter-

acting with the superconductor. We define the ground state as a stable state with the lowest energy. There are two possible stable states for the particle: vortex-like and single-domain states. We obtain a phase diagram (see Fig.3) where in the area above the phase boundary the ground state is vortex-like and below the boundary it is single-domain. Different curves on Fig.3 correspond to different values of λ_L .

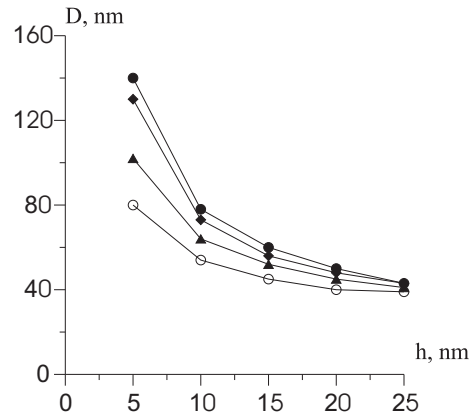


FIG. 3: Phase diagram of the vortex-single domain state transition. Filled circles- $\lambda_L = \infty$, open circles- $\lambda_L = 0$, triangles- $\lambda_L = 10nm$, rhombus- $\lambda_L = 50nm$.

Each phase boundary on Fig.3 has basic properties coming from the origin of phase transitions in a ferromagnetic nanoparticle¹⁵. They are determined by the interplay between the magnetostatic and exchange energy. In relatively large particles the ground state is vortex-like. When the dimensions (diameter D or height h) of the particle are reduced then the single domain state becomes the ground one. The superconductor influence shows up through an enlargement of the area of small-sized particles having the vortex-like state. It is clear that the shift of the phase boundary in comparison to the case $\lambda = \infty$ depends on the ratio of the interaction energy to the self-energy of the single-domain particle: E_{int}/E_0 . Since this ratio is very small $E_{int}/E_0 = 0.02 \ll 1$ at $\lambda_l = 50nm$, the phase boundary remains almost unchanged.

But the phase boundary between the two ground states is not important because at the large area around this curve on the phase diagram both the single domain and the vortex-like states are stable. When we cross the phase boundary from a large size to a smaller one, the vortex-like state becomes metastable, i.e., it is not the ground state but it does not transform to the single-domain state. This is also true for the single-domain state. The example of the area of metastability is shown on Fig.4.

Thus it is more important to investigate the boundary between the area of metastability and the absolute instability of the vortex-like or the single-domain state. This boundary depends on the external magnetic field \mathbf{H}_0 . It was found out that applying the in-plane field \mathbf{H}_0 we can cause nucleation of the vortex, i.e., make the single-domain state unstable, annihilation of the vortex,

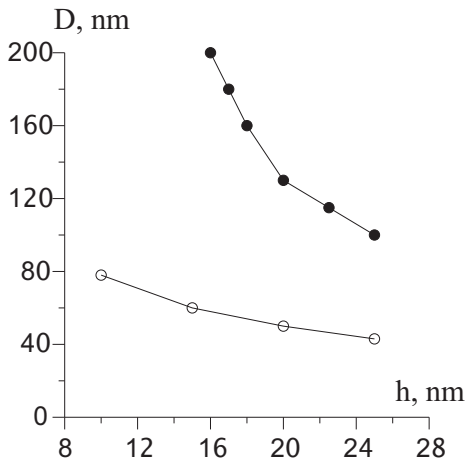


FIG. 4: Example of the metastability area (between the curves) of the vortex-like state. The upper curve (filled circles) is the boundary of the vortex-like state stability region, the lower curve (open circles) is the phase boundary between the vortex-like and single-domain ground states.

i.e. make the vortex-like state unstable^{8,9}. Practically, it is more convenient to vary the external magnetic field than the dimensions of the particle. That is why we investigate the vortex annihilation, H_{ann} (Fig.5) and nucleation, H_{nucl} (Fig.6) fields as functions of particle diameter D . The height of the particle is fixed: $h = 20nm$.

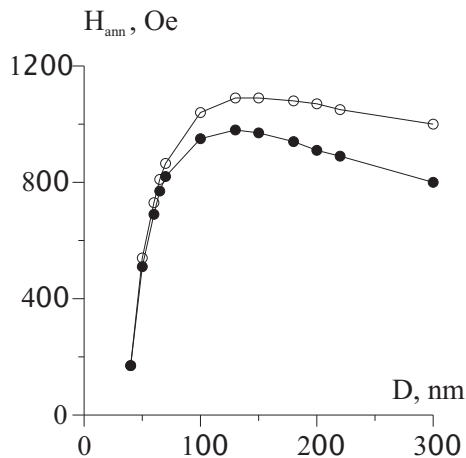


FIG. 5: The critical field H_{ann} of vortex annihilation as a function of diameter D . The height of the particle $h = 20nm$. The curve marked with filled circles is for $\lambda_L = \infty$, with open circles- for $\lambda = 50nm$.

The nucleation and annihilation of the vortex are parts of the process of magnetization reversal in a particle driven by the external magnetic field. If the particle is initially found in the single-domain state, then by applying external field \mathbf{H}_0 in the opposite to the magnetic moment direction we first stimulate a transition to the vortex-like state, i.e., nucleation of the vortex. When we increase the external field further, the vortex annihilates and the particle comes to the single-domain state again

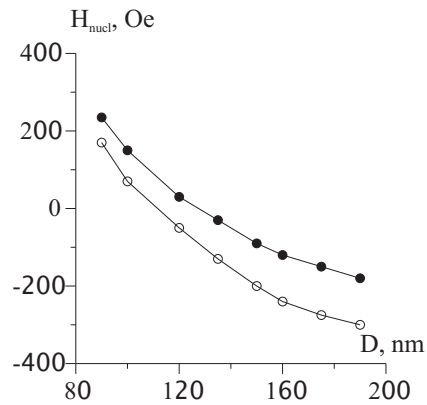


FIG. 6: The critical field H_{nucl} of vortex nucleation as a function of diameter D . The height of the particle $h = 20nm$. The curve marked with filled circles is for $\lambda_L = \infty$, with empty circles- for $\lambda = 50nm$.

but with a reversed magnetic moment. Note that the annihilation field H_{ann} as always positive for the particle with $h = 20nm$ (see Fig.5). The nucleation field H_{nucl} becomes negative when the diameter D is large enough (see Fig.6). This means that the single domain state is unstable and the external field should be applied in order to prevent the nucleation of the vortex-like state. In more detail we investigate the magnetization reversal for a particle of $D = 100nm$ and height $h = 20nm$. At the zero field the particle is in the single-domain state with an average magnetic moment directed along the x axis. The external field is applied in the opposite direction to the initial magnetic moment. The magnetization curve for this particle is shown on Fig.7(1). This curve describes the dependence of the average x -component of the magnetic moment M_x on the external magnetic field. The distribution of magnetization at the stages of the magnetization reversal process is shown on Fig.7(2).

The influence of a superconductor shows up in the reduced value of the average magnetic moment, because it decreases the interaction energy E_{int} . Therefore, the nucleation field for the particle placed above the superconductor is smaller and the annihilation field is larger than for the particle in the absence of superconductor. The difference between these fields increases with the size of the particle (see Fig.5, 6). When the diameter is quite large: $D > 100nm$, the shift of the nucleation and annihilation fields is about $100 - 200oe$. As we have noted before, this shift should be of order of the field produced by the superconducting current \mathbf{B}_s . To verify our results we find $\langle \mathbf{H}_s \rangle$ averaged over the z coordinate: $\langle \mathbf{H}_s \rangle (x, y) = \int_0^h \mathbf{H}_s(x, y, z) dz / h$. For an example we take a single-domain particle with $D = 100nm$ and $h = 20nm$. On Fig.8(a),(b),(c) we show the components of $\langle \mathbf{H}_s \rangle$ inside the particle. The magnetic field is normalized to the saturation magnetization $M_s = 800Oe$.

The x -component of magnetic field $\langle \mathbf{H}_s \rangle$ is the largest and it varies from $0.12M_s \approx 100Oe$ at the center

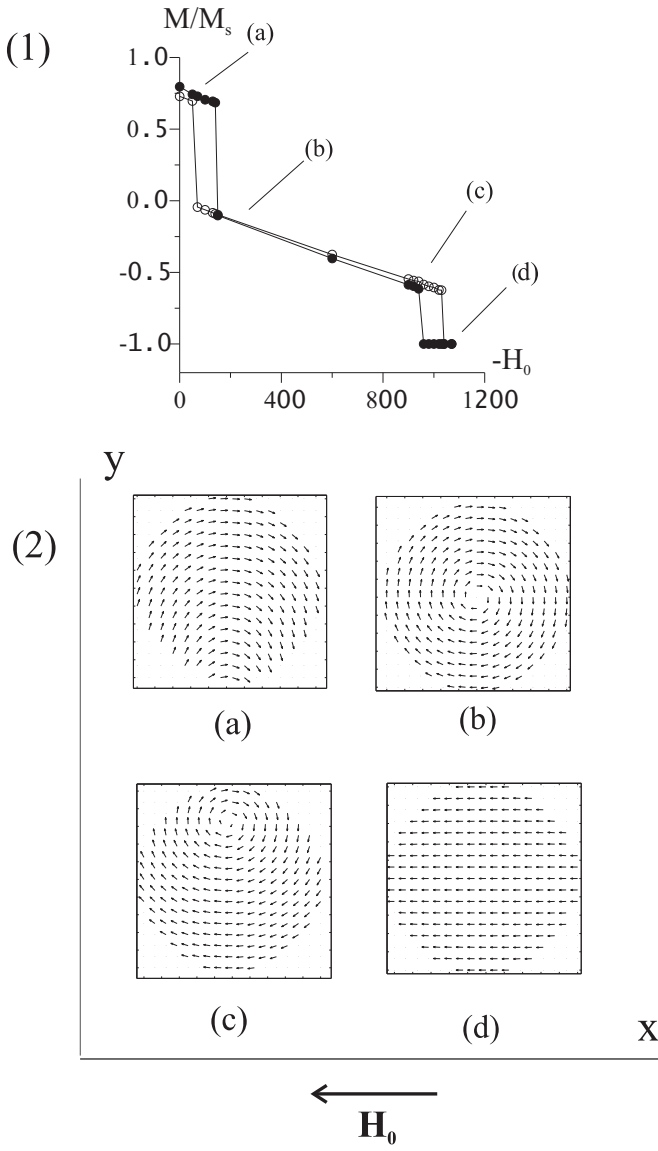


FIG. 7: (1) The process of magnetization reversal for $\lambda_L = \infty$ (open circles) and $\lambda_L = 50\text{nm}$ (filled circles). The particle dimensions are $h = 20\text{nm}$, $D = 100\text{nm}$, (a),(d)-single-domain states, (b),(c)-vortex-like state. (2) The evolution of magnetization distribution during the process of magnetization reversal.

of the particle to $0.06M_s \approx 50\text{Oe}$ at the edges. Thus ΔH_{nucl} and ΔH_{ann} should be about $50 \div 100\text{Oe}$. According to the results of simulation, the shift of the nucleation field for the cylindrical particle with $D = 150\text{nm}$ is $\Delta H_{nucl} = 110\text{Oe}$ (see Fig.6) and the shift of the annihilation field is $\Delta H_{nucl} = -120\text{Oe}$ (see Fig.5). Therefore, our estimation gives the right order of ΔH_{ann} and ΔH_{nucl} .

Let us now consider some possible experimental investigations based on the effects which we have described. Placing a ferromagnetic particle with diameter $D = 100 - 200\text{nm}$ and height $h = 20\text{nm}$ above the superconductor and cooling it below its critical temper-

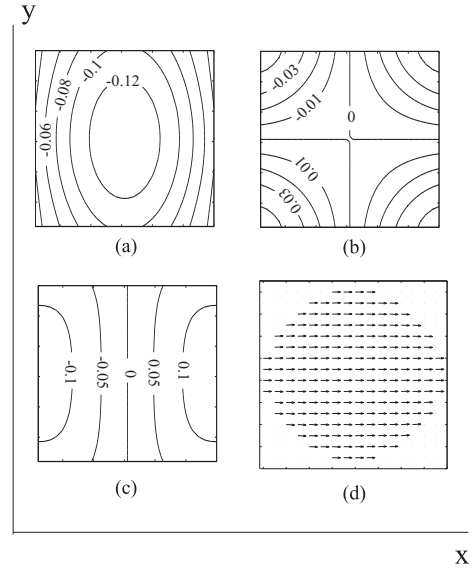


FIG. 8: (a)-(c) The level curves for the components $\langle H_{sx} \rangle$, $\langle H_{sy} \rangle$, $\langle H_{sz} \rangle$ of the magnetic field produced by the superconducting current. (d)-magnetization of the particle. $D = 150\text{nm}$, $h = 20\text{nm}$, $\lambda_L = 50\text{nm}$.

ature T_c we will have well observable shifts ΔH_{nucl} and ΔH_{ann} of about $100 - 200\text{Oe}$. Moreover, the shift of the annihilation field ΔH_{ann} enables us to realize a selective magnetization reversal in an array of ferromagnetic particles placed above the superconductor. If we neglect the interparticle interaction, then the magnetization curve of each particle is like the one shown on Fig.7.

Let us assume that initially all particles in the array are in the vortex-like state. Applying the magnetic field of magnitude between $H_{ann}(T < T_c)$ and $H_{ann}(T > T_c)$ (see Fig.9(1)) will lead to a reversible displacement of the vortex core within each particle (see Fig.9(2a)). If then we destroy the superconductivity around one of the particles, it will immediately fall into the single-domain state (see Fig.9(2b)). By removing the magnetic field we will have all particles get back to the initial state except for the one which will remain in the single-domain state. Thus we can operate with a single particle in an array without disturbing the state of other particles.

V. CONCLUSION

We presented the results of the numerical investigation of the magnetization reversal process in an external magnetic field of a ferromagnetic particle placed above the surface of a superconductor. The numerical simulation is based on solving the Landau-Lifshitz-Gilbert equation for the dynamics of magnetic moment. The superconductor is in the Meissner state and the only parameter that affects the interaction between the particle and the superconductor is the London penetration depth λ_L .

We have shown that for a realistic value of $\lambda_L = 50\text{nm}$

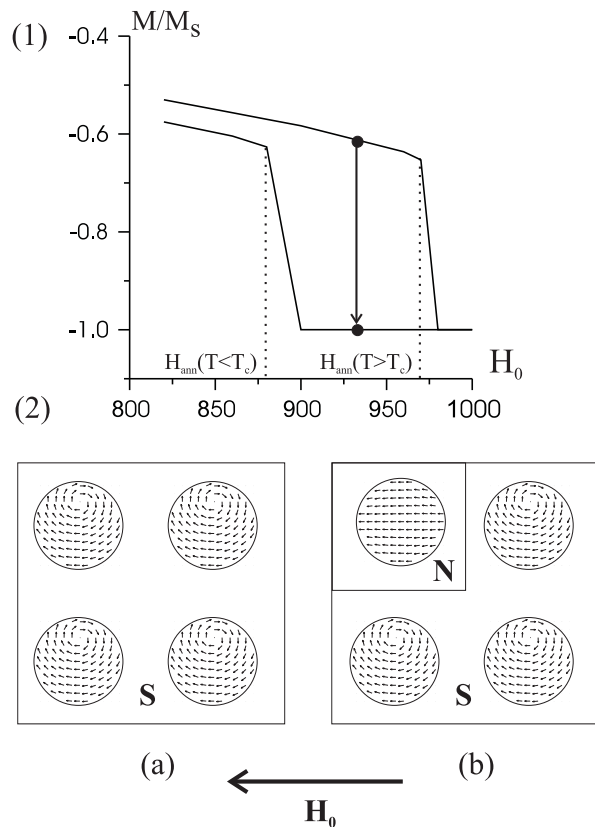


FIG. 9: (1)-Part of the magnetization curve near the annihilation of the vortex. (2)-Selective magnetization reversal in an array of ferromagnetic particles.

the interaction energy is much smaller than the self-energy of the particle and the ground state of the particles does not change significantly. But nevertheless, the magnetic field generated by the superconducting current leads to a decrease of the nucleation field and to an increase of the annihilation field by 100 – 200 Oe. Based on the effect of the annihilation field shift when the superconductor is cooled to temperatures below T_c we describe the method of a selective magnetization reversal in an array of ferromagnetic particles.

Acknowledgments

This work was supported by the Russian Foundation for Basic Research, Grant No. 03-02-16774 and Materials Theory Institute at the Argonne National Laboratory.

-
- ¹ S. Tehrani, E. Chen, M. Durlam, M. DeHerrera, J. M. Slaughter, J. Shi, and G. Kerszykowski, *J. Appl. Phys.* **85**, 5822 (1999).
- ² S. Y. Chou, *Proc. IEEE* **85**, 652 (1997).
- ³ C. A. Ross, H. I. Smith, T. Savas, M. Schattenburg, M. Farhoud, M. Hwang, M. Walsh, M. C. Abraham, and R. J. Ram, *J. Vac. Sci. Technol. B* **17**, 3168 (1999).
- ⁴ R. P. Cowburn, D. K. Koltsov, A. O. Adeyeye, and M. E. Welland, *J. Appl. Phys.* **87**, 7082 (2000).
- ⁵ A. M. Kosevich, M. P. Voronov, I. V. Manzhos, *Zh. Exp. Teor. Fiz.* **52** 148 (1983)
- ⁶ Y. Ishii, Y. Nakazava, *J. Appl. Phys.* **81** 1847 (1996)
- ⁷ A. Aharoni, *J. Appl. Phys.* **68**, 2892 (1990)
- ⁸ K. Yu. Guslienko, V. Novosad, Y. Otani, H. Shima, and K. Fukamichi, *Phys. Rev. B* **65**, 024414 (2001)
- ⁹ A. A. Fraerman, S. A. Gusev, L. A. Mazo, I. M. Nefedov, Yu. N. Nozdrin, I. R. Karetnikova, M. V. Sapozhnikov, I. A. Shereshevskii, and L. V. Sukhodoev, *Phys. Rev. B* **65**, 064424 (2002)
- ¹⁰ E. B. Sonin *Phys. Rev. B* **66**, 136501 (2002)
- ¹¹ L. N. Bulaevskii and E. M. Chudnovsky, *Phys. Rev. B* **63**, 012502 (2000)
- ¹² S. V. Dubonos, A. K. Geim, K. S. Novoselov, and I.V. Grigorieva, *Phys. Rev. B* **65**, 220513(R) (2002)
- ¹³ M. J. Van Bael, J. Bekaert, K. Temst, L. Van Look, V. V. Moshchalkov, Y. Bruynseraede, and G. Borghs, *Phys. Rev. Lett.* **86**, 155 (2001)
- ¹⁴ A. A. Fraerman, I. R. Karetnikova, I. M. Nefedov, A. V. Sapozhnikov, and I. A. Shereshevskii, *The Physics of Metals and Metallography* **92**, S226 (2001)
- ¹⁵ R. P. Cowburn and M. E. Welland, *Appl. Phys. Lett.* **72**, 2041 (1998)
- ¹⁶ Serkan Erdin, Amin F. Kayali, Igor F. Lyuksyutov, and Valery L. Pokrovsky, *Phys. Rev. B* **66**, 014414 (2002)